Electronic Supplementary Material (ESI) for Journal of Materials Chemistry A.

Supplementary Information:
Toward “Rocking-chair type” Mg-Li Dual-salt Battery

Shinya Okamoto,[1] Tetsu Ichitsubo,[1*] Tomoya Kawaguchi,[1] Yu Kumagai,[2] Fumiyasu Oba,[1,2]
Shunsuke Yagi,[3] Natsumi Goto,[1] Takayuki Doi,[4] Eiichiro Matsubara[1]

Determination of the conversion rules of the Mg and Li redox potentials

Through the present work, binary or ternary ionic liquids composed of $Mg(TFSA)_2$, LiTFSA, and CsTFSA were used as electrolytes, where TFSA is bis(trifluoromethanesulfonyl)amide, $N(CF_3SO_2)_2{}^-$.[1,2] The melting points of CsTFSA and LiTFSA are 122°C, and 233°C, respectively,[3] and $Mg(TFSA)_2$ has no melting point due to the decomposition of the TFSA anion molecules. Hence, the addition of CsTFSA drastically decreases the melting point of the mixed salt of $Mg(TFSA)_2$, LiTFSA, and CsTFSA, which enables us to use the molten salt at 150°C.

Although the electrodeposition of Mg is hardly detected in the binary $Mg(TFSA)_2$-CsTFSA ionic liquid, the electrodeposition of Mg can be detected in the presence of LiTFSA. In what follows, a Li metal immersed in 0.5 M LiTFSA/DEMETFSA (N,N-diethyl-N-methyl-N-(2-methoxyethyl)ammonium bis(trifluoromethanesulfonyl)amide) electrolyte, which was separated in a glass tube with ceramic filter, was used as the reference electrode (RE), because Mg metal was readily passivated in the ionic liquids and the potential of Mg metal gradually shifts to higher values possibly due to the reaction with TFSA.[2] To convert the measured potentials vs. Li^+/Li in RE to those vs.

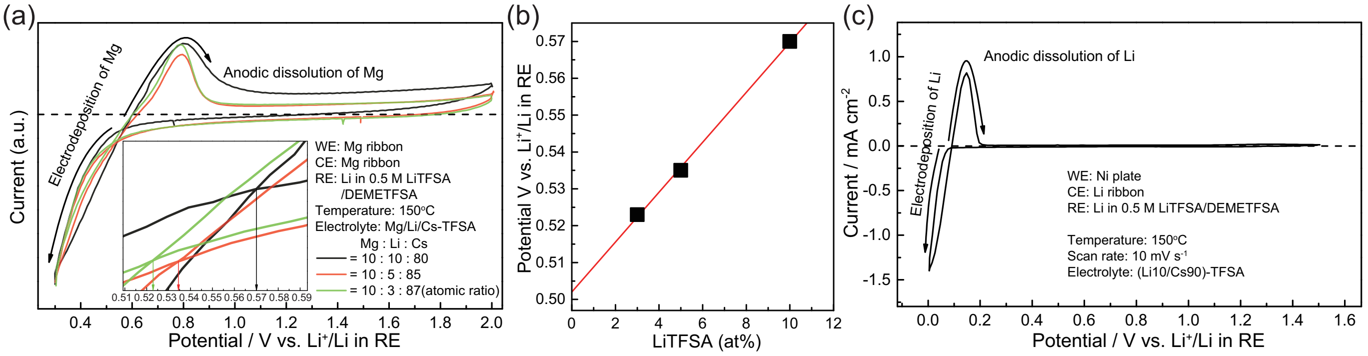

FIG. S1: (a) Cyclic voltammogram measured at 150°C in the ionic liquid of the mixture of $Mg(TFSA)_2$, LiTFSA, and CsTFSA salts with various concentrations. The concentration of $Mg(TFSA)_2$ was fixed at 0.10 M, and the fraction of LiTFSA and CsTFSA was changed. The working electrode (WE) and counter electrode (CE) were polished Mg metals and the reference electrode (RE) was a Li metal in the LiTFSA immersed in the DEMETFSA solvent. (b) Redox potential of the Mg^{2+}/Mg couple plotted to the LiTFSA concentration in the electrolyte. (c) Cyclic voltammogram measured at 150°C in the (Li10/Cs90)-TFSA ionic liquid. The working electrode (WE) and counter electrode (CE) were polished Ni metal and Li metal, respectively, and the reference electrode (RE) was a Li metal in the LiTFSA immersed in the DEMETFSA solvent.

---

[*] Corresponding: tichi@mtl.kyoto-u.ac.jp

Mg^{2+}/Mg, the redox potential of the Mg^{2+}/Mg couple was electrochemically measured in the ternary ionic liquids with various concentrations of LiTFSA. Figure S1(a) shows the cyclic voltammograms measured at 150°C in the ionic liquids, whose molar fraction is $Mg(TFSA)_2$:LiTFSA:CsTFSA $= 10{:}x{:}(100-x)$, where $x = 3, 5$, and 10. Below and above about 0.6 V vs. Li^+/Li in RE, the cathodic current for Mg electrodeposition and the anodic current for Mg dissolution are clearly seen in all the Li compositions. The redox potential of the Mg^{2+}/Mg couple can be determined to be the crossover point of the current. As shown in Fig. S1(b), approximately there is a linear relationship between the redox potential of the Mg^{2+}/Mg couple and the concentration of LiTFSA. By extrapolating the fitted line to the zero concentration point of LiTFSA, the redox potential of the Mg^{2+}/Mg couple was estimated to be about 0.5 V vs. Li^+/Li in RE in the binary (Mg10/Cs90)-TFSA ionic liquid ($Mg(TFSA)_2$:CsTFSA=1:9 in molar fraction).

On the other hand, Fig. S1(c) shows the cyclic voltammogram measured at 150°C in the (Li10/Cs90)-TFSA ionic liquid, which shows that the redox potential of Li^+/Li couple is about 0.1 V vs. Li^+/Li in RE.

Thus, in the manuscript, the potential vs. Mg^{2+}/Mg or that vs. Li^+/Li converted using these relationships is also indicated in the upper horizontal axis of the figures.

Cyclic voltammograms of Magnesium Cobaltate

Figure S2 shows the cyclic voltammograms (CVs) of $MgCo_2O_4$ for Mg and Li insertion/extraction processes. Usually, one would consider the conventional reaction, i.e., the reaction of Mg extraction from the host material, $MgCo_2O_4 \leftrightarrow Mg_{1-x}Co_2O_4 + x(Mg^{2+} + 2e^-)$. However, as seen in Fig. S2(a), this reaction would occur above 4.4 V vs. Li^+/Li in RE but this cation extraction from $MgCo_2O_4$ is quite faint, so that it would be difficult to obtain a sufficient capacity. Apart from this usual deintercalation, it is clearly seen that direct Mg insertion can occur into the host $MgCo_2O_4$ (even without a pre-charge process), and then the cation extraction during a charge process is reversibly observed (incidentally, Cs cations can hardly be inserted into $MgCo_2O_4$). The equilibrium redox potential

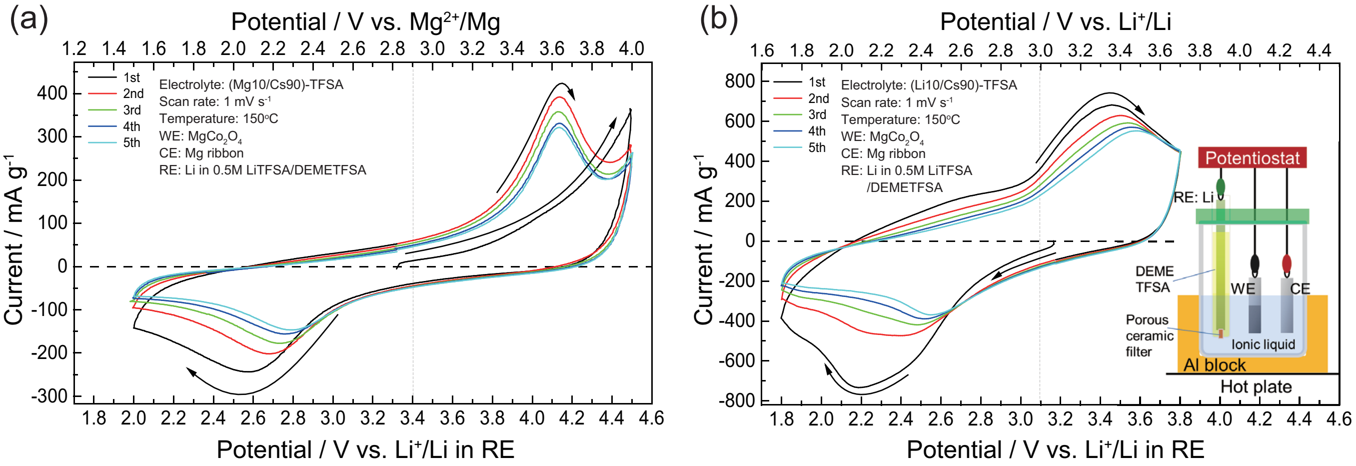

FIG. S2: Cyclic voltammograms of $MgCo_2O_4$ at 150°C for (a) Mg and (b) Li insertion/extraction processes. The ionic liquids of $Mg(TFSA)_2$:CsTFSA = 1:9 and LiTFSA:CsTFSA = 1:9 (mol ratio) were used for the Mg battery and the Li battery, respectively. The inset in (a) shows a spinel structure, where a 32e site is set at origin. The inset in (b) illustrates a typical three-electrode beaker cell used in the present work, where Li metal immersed in a 0.5 M-LiTFSA/DEMETFSA electrolyte in a glass tube separated with a porous ceramic filter was used as the reference electrode (RE).

is estimated to be as high as about 2.9 V vs. Mg^{2+}/Mg (3.4 V vs. Li^+/Li in RE). As before, a usual problem in MRBs is the sluggish diffusion of Mg^{2+} cations at ambient temperature due to strong coulomb restraint in the crystal, but the insertion/extraction of Mg cations are found to be drastically facilitated by slightly elevating temperature; the working-temperature dependence for $MgCo_2O_4$ will be discussed later. In addition, Li insertion/extraction also occurs for $MgCo_2O_4$, as seen in Fig. S2(b), whose redox potential is evaluated to be about 3.1 V vs. Li^+/Li (3.2 V vs. Li^+/Li in RE); see Fig. S1 for the potential conversion rule. Thus, the insertion potential of Li is found to be slightly lower than that of Mg, but the current density for Li is 2-3 times higher than that for Mg, which would contribute to a higher power density in DSB systems.

Other candidates of electrolyte

In order to show the generality of anode morphology after charge in the Mg/Li dual-salt battery, we present the results obtained by use of triglyme solution. Figure S3 shows cyclic voltammograms measured in two kinds of triglyme electrolytes: dual-salt electrolyte containing 0.5 M LiTFSA and 0.5 M $Mg(TFSA)_2$ and single-salt electrolyte containing only 0.5 M LiTFSA.[4] Both the cyclic voltammograms show that Li metal is deposited below about 0 V vs. Li^+/Li.

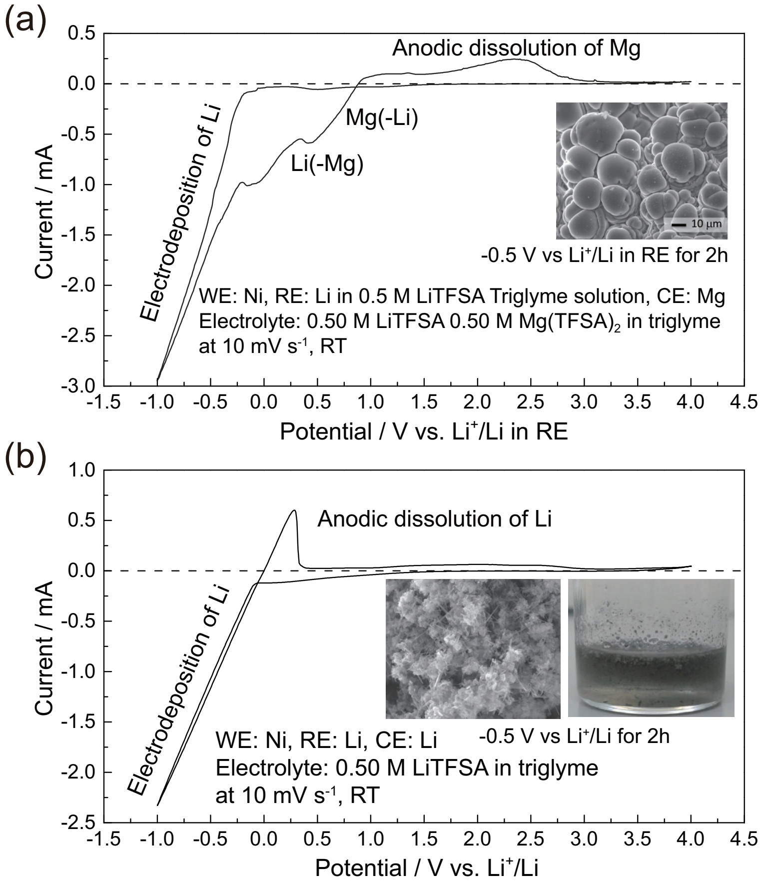

FIG. S3: Cyclic voltammograms measured at 10 mV s^{-1} and room temperature in (a) triglyme electrolyte containing 0.5 M LiTFSA and 0.5 M $Mg(TFSA)_2$ and (b) 0.5 M LiTFSA. SEM micrographs of the deposit obtained at -0.5 V vs. Li^+/Li for 2h are also shown in the insets.

However, the surface morphology of the Li deposit obtained at -0.5 V vs. $\mathrm{Li^+/Li}$ for 2h is totally different; see SEM photographs in Fig. S3. No dendrites are observed in the Li(-Mg) deposit from the LiTFSA-Mg(TFSA)$_2$/triglyme dual-salt electrolyte, which is owing to the co-deposition or alloying with Mg. In contrast, dendrites of Li is clearly observed in the deposit from the 0.5 M LiTFSA/triglyme electrolytesingle-salt electrolyte, resulting in Li segments fallen-off in the beaker. Thus, we have confirmed the common feature of anode morphology in the Mg/Li dual-salt systems, that is, the non-dendritic morphology can be attained not only in Grignard-reagent/tetrahydrofuran electrolyte[5] and the present ionic liquids but also in TFSA-salt/triglyme electrolyte. Thus, alloying of Li with Mg suppresses the formation of dendrites irrespective of the electrolytes, which is one of the most superior advantages in the Mg/Li dual-salt battery system.

On the cyclability

In Figs. 2e and 2f, the reversible capacity gradually fades with cycle numbers; however, this would not be due to the degradation of the active material. In order to investigate what lowers the cyclability, we investigated the morphology change in the composite electrode composed of $\mathrm{MgCo_2O_4}$ (active material), carbon black (conductive agent), and PVDF (binder) at a weight percent of 80:10:10. Fig. S4 shows the SEM images of the $\mathrm{MgCo_2O_4}$ composite electrode before and after the 4 cycles of the charge-discharge test in the binary ionic liquid of (Mg10/Cs90)-TFSA at 130 °Cwhich is below the present operating temperature, 150 °C. As seen in Fig. S4, the composite electrode is relatively smooth and flat before the test. In contrast, many voids or fracture are observed after the test, which is possibly due to the melting and/or dissolution of the PVDF binder (even at 130 °C). The existence of the voids can cause

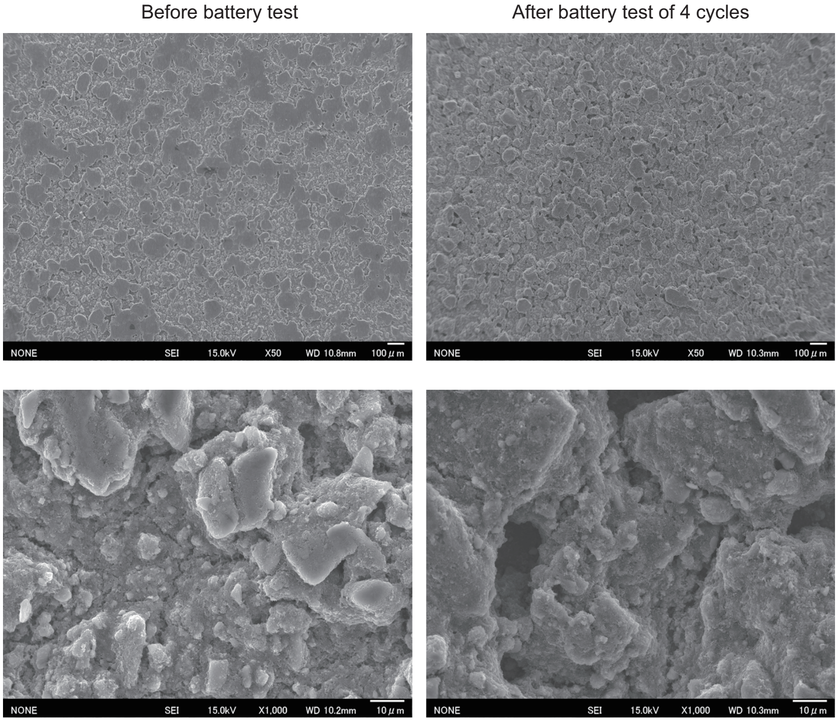
Before battery test
After battery test of 4 cycles

FIG. S4: SEM images of the $\mathrm{MgCo_2O_4}$ composite electrode before and after the 4 cycles of the charge-discharge test in the binary ionic liquid of (Mg10/Cs90)-TFSA at 130 °C.

the lowering of the conductivety and detachment of the active material. Therefore, it is necessary to establish more stable binders to enhance the cyclability.

Electrode characteristics in a Mg/Li dual salt battery system

Chemical compositions of cathode and anode materials by ICP analysis

Chemical compositions of cathode and anode materials were measured by ICP (Inductively Coupled Plasma) analysis. Samples presented here corresponds to Figs. 1 and 2 in the body text, where the DSB system was demonstrated. We have obtained the respective compositions for as-synthesized $MgCo_2O_4$, one after battery test in Fig. 2**f**, Mg-Li alloy initial composition used as an anode material, and composition of Mg-Li alloy electrodeposited in the DSB system using (Li10/Mg10/Cs80)-TFSA (cation atomic ratio: Li/Mg/Cs = 10/10/80) ternary ionic liquid in Fig. 1 (lower right). As seen in Table S1, since the electrode was set at such a sufficiently low potential as Li metal can be electrodeposited, the alloy was composed of mainly Li (about 62%) and Mg (about33%), including a small amount of Cs (about 5%). Nevertheless, the dendritic formation was shown to be significantly suppressed in the anode morphology. In addition, since Cs is the most non-noble between three cations, the electrodeposited alloy contained few amount of Cs, and the contamination of Cs would hardly affect the morphology of the Mg-Li alloy system in terms of phase-separation characteristics in the phase diagrams of Cs-Mg and Cs-Li systems.

TABLE S1: ICP analysis of electrodes; all compositions are represented by atomic percent.

Sample \ Element	Li	Mg	Co	Cs	Na	Normalized	Li	Mg	Co	Cs	Na	Corresponding
As-synthesized $MgCo_2O_4$	—	31.6	68.2	—	0.2	by Co	—	0.9	2	—	0.0	Fig. 2**f**
After the final discharge in DSB	11.9	38.0	47.5	2.6	—	by Co	0.5	1.6	2	0.1	—	Fig. 2**f**
Initial composition Mg-Li alloy for DSB	51.0	49.0	—	—	—	by Mg	1.0	1	—	—	—	Fig. 2**f**
Alloy deposited at -0.5 V[a] in DSB	61.4	33.2	—	5.4	—	by Mg	1.9	1	—	0.2	—	Fig. 1

[a] The potential is based on vs. Li^+/Li in RE.

Anodic-dissolution potential of the counter electrode during charge/discharge

Figure S5 shows the potential of the working electrode (WE) and the counter electrode (CE) during the battery test for Mg/Li dual-salt battery system (three-electrode beaker cell), corresponding to Fig. 2**f** in the body text. During the discharge, the anodic dissolution of the BCC Li-Mg alloy ($Mg_{50}Li_{50}$ at atomic ratio) at CE occurs at about 0.5–0.6 V vs. Li^+/Li in RE. On the other, the CE potential during charge is about 0.25 V vs. Li^+/Li in RE, and hence Mg would be mainly deposited due to the presence of inexhaustible Mg ions in the beaker cell (thus, in this case, through cycles of charge and discharge, Mg would be gradually concentrated in the Mg-Li alloy). What is the most important in the present experiments is that the CE potential during discharge (i.e., the anodic dissolution) is not fluctuated, suggesting that the Mg-Li alloy is stable and substantially free from the macroscopic passivation.

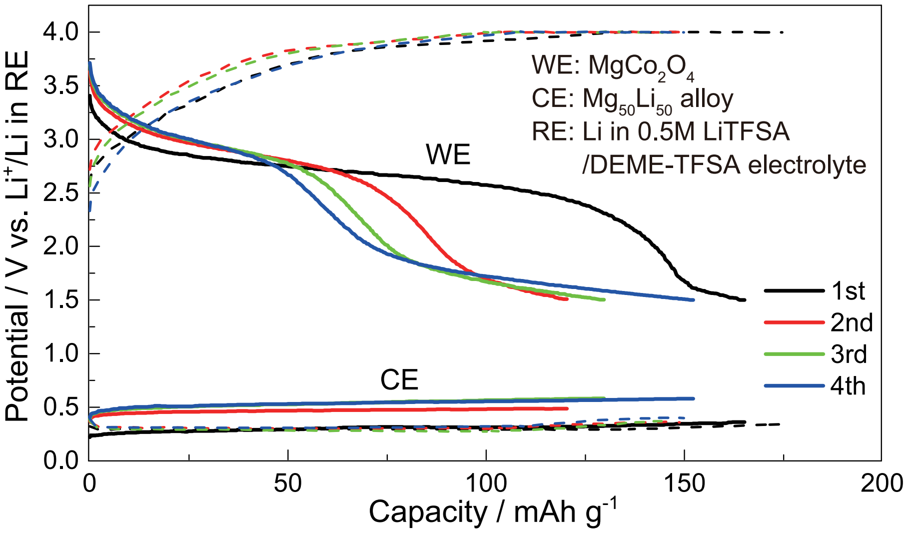

FIG. S5: Battery cycle test for the Mg/Li dual-salt battery system at 150°C, WE: $MgCo_2O_4$, CE: Mg-Li alloy ($Mg_{50}Li_{50}$ at atomic ratio), RE: Li in a separate glass tube, electrolyte: ternary ionic liquid of LiTFSA:Mg$(TFSA)_2$:CsTFSA = 10:10:80 (mole percent). The C rate was set at 1/12 C.

***Ab initio* calculations**

Determination of spin and magnetic configurations in spinel $MgCo_2O_4$.

We here discuss the stable spinel structure of $MgCo_2O_4$ before inserting Mg or Li cations. Since $MgCo_2O_4$ is a partially disordered spinel, the model has three degrees of freedom, i.e., the cation configuration, spin configuration, and magnetic configuration. Regarding the cation configuration, we considered all possible configurations in the primitive unit cell comprising 14 atoms, i.e., ${}_6C_2 = 15$ configurations, including symmetrically equivalent ones. For each atomic configuration, we searched for the most stable spin and magnetic configuration within the collinear magnetic configuration in the unit cell. In $MgCo_2O_4$, Co is trivalent, and can take high- or low-spin states at the tetrahedral or octahedral sites. Especially, it is well known that the energies of Co(III) high- and low-spin states at the octahedral sites, the latter of which has no local magnetic moment, are so close that both can exist depending on temperature in some materials. On the other hand, the high-spin state would be favorable for Co(III) at the tetrahedral sites. Therefore, we considered both high- and low-spin states for the octahedral sites, whereas only the high-spin state for the tetrahedral sites. In total, we calculated, for each atomic configuration, 10, 11, or 12 spin and magnetic configurations without considering symmetry, which includes one non-spin state, $2^3 = 8$ magnetic configurations for the high-spin state, and 0, 1, or 2 magnetic configurations for the mixed-spin state comprising low spins for the octahedral sites. As a result, it is found that the high-spin states are more stable than the other spin states except in one structure (No. 6 in Fig. S6), where the mixed-spin state is 0.2 eV lower in energy than the most stable high-spin state.

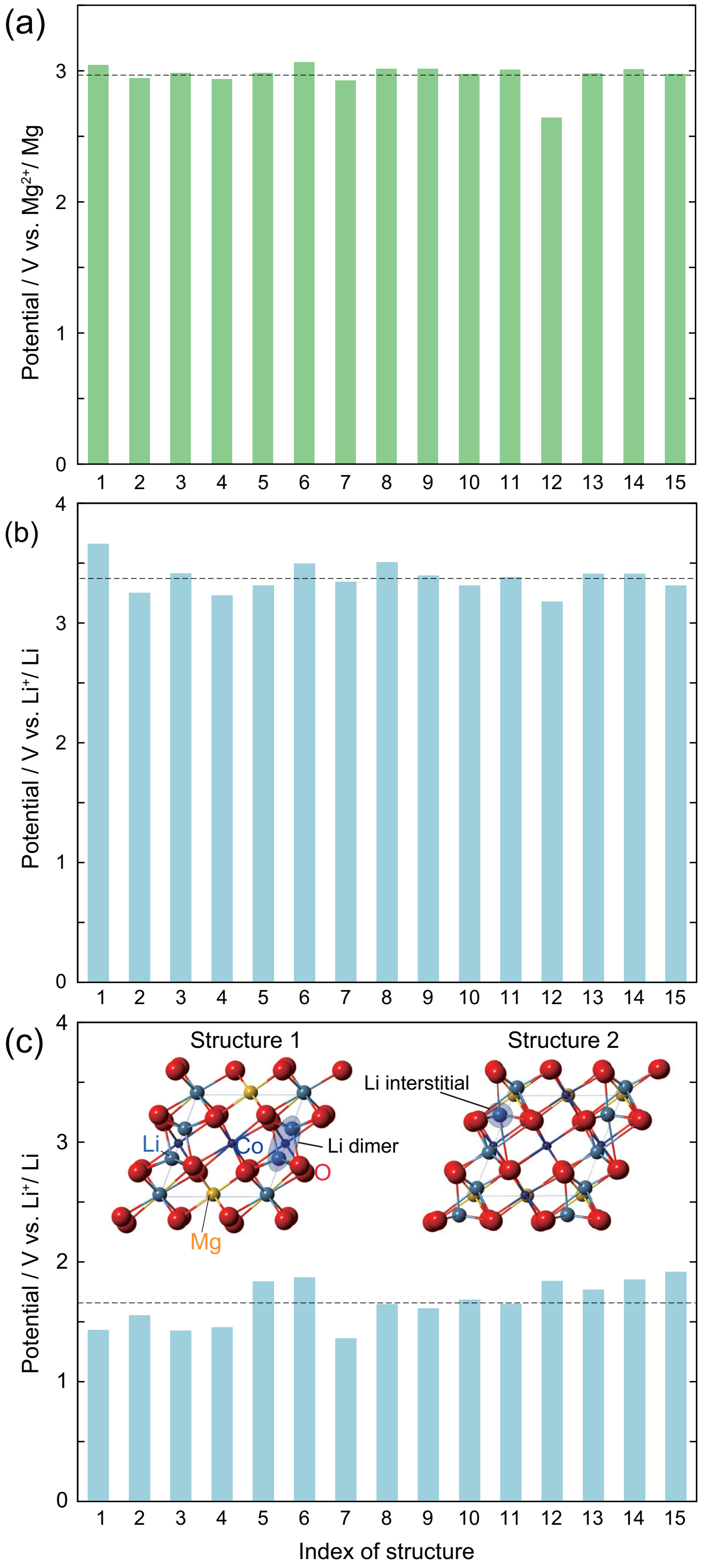

FIG. S6: Calculated redox potential of $MgCo_2O_4$ using GGA+U for all 15 possible atomic configurations in the spinel primitive unit cell by insertion of (a) Mg and (b) Li cations to compose $Mg_2Co_2O_4$ and $LiMgCo_2O_4$ in the rocksalt structure, respectively, and (c) by further insertion of Li cations in the range of $1 < x < 1.5$ in $Li_xMgCo_2O_4$. The insets show the relaxed atomic positions in structures 1 and 2. In structures No. 2, 10, and 11, the extra Li cations are located at the 8a sites surrounded by two Li cations (as structure 2 in the inset). In the other structures, they construct Li-Li dimers around 16c sites (as in structure 1 in the inset). The averaged redox potentials are shown with dashed lines.

Mg and Li insertion into spinel $MgCo_2O_4$.

Next let us discuss the structures and energetics of Mg/Li insertion into spinel $\mathrm{MgCo_2O_4}$. We calculated the redox potential V of $\mathrm{MgCo_2O_4}$ by insertion of Mg cations to give rise to the rocksalt structure as

$$V^{\mathrm{Mg}} = -\frac{1}{2e}[E(\mathrm{Mg_2Co_2O_4}) - E(\mathrm{MgCo_2O_4}) - E(\mathrm{Mg})],$$

and by insertion of Li cations as

$$V^{\mathrm{Li}} = -\frac{1}{e}[E(\mathrm{LiMgCo_2O_4}) - E(\mathrm{MgCo_2O_4}) - E(\mathrm{Li})],$$

where $e(>0)$ is the elementary charge and E denote the total energies of respective phases. Two Mg or Li cations were placed at the 16c sites in the primitive unit cell for each atomic configuration, and then the atomic positions and cell parameters were fully optimized. We started the structure optimization from two sets of initial atomic positions, i.e., with and without displacement of the 8a site cations into the 16c site. We considered only one cation configuration for each in the former set, since preliminary calculations indicated that the cation configuration in the rocksalt phase makes little impact on the redox potentials. Without the displacement, it has been found that some 8a cations spontaneously move to 16c sites but others do not, showing much higher energies compared to the rocksalt structures with the displacement. Subsequently, the most stable magnetic configuration was again determined for each atomic configuration. Since Co(II) is known to take the high-spin state at both of the tetrahedral and octahedral sites, we considered the high-spin state only. For Co(III) in $\mathrm{LiMgCo_2O_4}$, both high- and low-spin states were considered. As a result, the high-spin states are again more stable than the other spin states except in one structure (No. 1, with the normal spinel structure before Li insertion), where the mixed-spin state is 0.6 eV lower in energy than the most stable high-spin state. Using the total energies of the most stable magnetic configurations before and after inserting cations, we estimated redox potential for each atomic configuration as shown in Figs. S6a and b. The estimated redox potentials are almost irrelevant to the atomic configurations except for No. 12 in Fig. S6a, in which $\mathrm{Mg_2Co_2O_4}$ has a (100) ordered $\mathrm{L1_0}$ structure.

We also calculated the average redox potential by further insertion of Li cations in the (single-phase) range of $1 \le x \le 1.5$ in $\mathrm{Li}_x\mathrm{MgCo_2O_4}$ as

$$V_{\mathrm{ex}}^{\mathrm{Li}} = -\frac{1}{0.5e}[E(\mathrm{Li_{1.5}MgCo_2O_4}) - E(\mathrm{LiMgCo_2O_4}) - 0.5E(\mathrm{Li})].$$

We optimized the structures after setting the extra Li cations at the 8a site (Wyckoff positions based on the original spinel structures) near Li cations in the optimized rocksalt $\mathrm{LiMgCo_2O_4}$ structures. When the extra Li cation was set at the 8a site far from the original Li cations, the optimized structure showed a rather higher energy or the Li ion has moved to the vicinity of the original Li cations through the structure optimization. As shown in the insets of Fig. S6c, we have obtained two kinds of optimized structures; in some optimized structures, the extra Li cations have moved to form Li-Li dimers with the original Li cations, and in other structures, they are located at the 8a sites surrounded by two Li cations.

Besides, we also modeled $Li_2MgCo_2O_4$ by adding further Li ions at 8b (the other tetrahedral interstitial) sites. It is found that some cation configurations show significant atomic displacements and lattice distortions, and the redox potentials of other configurations keeping the rocksalt framework turned out to be negative. This indicates that Li insertion in high concentration close to $x = 2$ must be laborious.

---

[1] B. Gao, T. Nohira, R. Hagiwara and Z. Wang, Molten Salts Chemistry and Technology, M. Gaune-Escard and G. M. Haarberg eds., *John Wiley & Sons, Ltd.*, 2014, Chapt. 5.4.

[2] M. Oishi, S. Okamoto, T. Ichitsubo, S. Toyoda, E. Matsubara, T. Nohira and R. Hagiwara, *J. Electrochem Soc.*, 2014, **161**, A943–947.

[3] R. Hagiwara, K. Tamaki, K. Kubota, T. Goto, and T. Nohira, *J. Chem. Eng. Data*, 2008, **53**, 355–358.

[4] T. Fukutsuka, K. Asaka, A. Inoo, R. Yasui, K. Miyazaki, T. Abe, K. Nishio and Y. Uchimoto, *Chem. Lett.*, 2014, **43**, 1788-1790.

[5] S. Yagi, T. Ichitsubo, Y. Shirai, S. Yanai, T. Doi, K. Murase and E. Matsubara, *J. Mater. Chem. A*, 2014, **2**, 1144–1149.